Supporting Information

Projecto-Garcia et al. 10.1073/pnas.1315456110

SI Methods

Protein Purification. The HbA and HbD isoforms were separated by passing the samples through an ion-exchange chromatography column (HiTrap QHP, 5 × 1 mL, 17–1153-01; GE Healthcare) equilibrated with 20 mM Tris buffer (pH 8.2) and eluted using a linear gradient of 0–0.2 M NaCl. Samples were desalted by overnight dialysis against three changes of 10 mM Hepes buffer (pH 7.6) at 4 °C. Samples were concentrated (to >1 mM heme) using Millipore centrifugal filter units (MW = 30,000; Millipore) at 7,000 × *g* before freezing at −80 °C. Heme oxy concentration (millimolar) was calculated from the absorbance peaks in the visible region of the spectrum (577 nm and 540 nm) using standard extinction coefficients.

Hb-O_2 Equilibria. O_2-equilibrium curves were measured using a modified O_2 diffusion chamber where changes in absorption (436 nm) of ultrathin (~1.4 μm) layers of Hb solutions were recorded following complete oxygenation (100% saturation) and deoxygentation (0% saturation) of Hb, achieved via equilibration with pure O_2 and N_2, respectively, and complete equilibration to gas mixtures of varying O_2 tension generated by precision Wösthoff gas-mixing pumps, as described previously (1–3). Values of P_{50} and n_{50} (Hill's cooperativity coefficient at half-saturation) were interpolated from the linear portion of Hill plots [log ([HbO_2]/[Hb] vs. log PO_2] based on four to six equilibration steps between 30% and 70% oxygenation. Free Cl^- concentrations were measured with a model 926S Mark II chloride analyzer (Sherwood Scientific). We used standard concentrations of Cl^- (0.1 M KCl) and inositol hexaphosphate (IHP; IHP/Hb tetramer ratio = 2.0) (4, 5) that closely approximate intraerythrocytic effector concentrations in vivo (6–8). Predicted P_{50}s of composite hemolysates were calculated as the average value for HbA and HbD, weighted according to the naturally occurring relative concentration of each isoform.

Vector Construction and Site-Directed Mutagenesis. The α^A- and β^A-globin genes of *Adelomyia melanogenys* were synthesized by Genscript after optimizing nucleotide sequences with respect to *Escherichia coli* codon preferences. Gene cassettes for the α^A- and β^A-globin genes and the *methionine aminopeptidase* (*MAP*) gene were tandemly cloned into the custom pGM expression plasmid described by Natarajan et al. (9). To maximize efficiency in the posttranslational cleaving of N-terminal methionines from the α- and β-chain polypeptides, an additional copy of the *MAP* gene was cloned into the pCO-MAP plasmid with a kanamycin resistant gene and was coexpressed with the pGM expression plasmid.

The *A. melanogenys* β^A-globin was converted into the *Oreotrochilus estella* sequence by engineering two codon changes (β13Gly→Ser and β83Gly→Ser) using site-directed mutagenesis. The same procedure was used to engineer the two possible mutational intermediates between the β-chain Hbs of the two species (β13Ser-β83Gly and β13Gly-β83Ser). The mutagenesis experiments were performed with the QuikChange II XL Site-Directed Mutagenesis kit from Stratagene in accordance with the manufacturer's protocol. The presence of each engineered codon change was verified by DNA sequencing. In addition to the two above-mentioned β-chain substitutions, the major Hb isoforms of *A. melanogenys* and *O. estella* are also distinguished from one another by a single conservative α-chain substitution. We retained the *A. melanogenys* character state at this site (α8Thr) in all engineered rHbs to control for the effects of substitutions at β13 and β83.

Expression, Purification, and Functional Analysis of Recombinant Hemoglobins. All recombinant hemoglobins (rHbs) were expressed in the JM109 (DE3) *E. coli* strain and the bacterial cells were subject to dual selection in an LB agar plate containing ampicillin and kanamycin to ensure that the transformants receive both the pGM and pCO-MAP plasmids. Large-scale production was conducted in 1- to 1.5-L batches containing TB medium. Cells were grown at 37 °C in an orbital shaker at 200 rpm until absorbance values reached 0.6–0.8 at 600 nm. The cells were induced with 0.2 mM isfopropyl-β-D-thiogalactopyranoside (IPTG) and were then supplemented with hemin (50 μg/mL) and glucose (20 g/L). The cells were then subsequently grown at 28° C for 16 h in an orbital shaker at 200 rpm. The bacterial culture was saturated with CO for 15 min and the cells were harvested by centrifugation and stored at −80 °C. Subsequently the cells were resuspended in lysis buffer (3 mL/g of cells, 50 mM Tris base, 1 mM EDTA, 0.5 mM DTT) and lysozyme (1 mg/g cells) was added before sonication. Polyethyleneimine solution (0.5–1%) was added to the crude lysates to precipitate nucleic acids. After centrifugation (15,000 × *g* for 45 min at 4 °C), the clarified supernatants were dialyzed overnight against three changes of 20 mM Tris buffer (0.5 mM EDTA, 0.5 mM DTT, pH 7.6) at 4 °C. Centrifugation at 14,000 × *g* was used to pellet cell debris. Recombinant Hbs were then purified in a two-step process using ion-exchange chromatography. In the first step, the sample was passed through a column (HiTrap SPHP, 5 × 5 mL, 17–1152-01) equilibrated with 20 mM Tris buffer (0.5 mM EDTA, 0.5 mM DTT, pH 6.0) and was eluted using a linear gradient of 0–0.5 M NaCl. In the second step the sample was passed through another ion-exchange column (HiTrap QHP, 5 × 5 mL, 17–1153-01; GE Healthcare) equilibrated with 20 mM Tris buffer (0.5 mM EDTA, 0.5 mM DTT, pH 8.5) and was eluted using a linear gradient of 0–0.5 M NaCl. Samples were desalted by overnight dialysis against three changes of 10 mM Hepes buffer (pH 7.6) at 4 °C. If necessary, samples were concentrated to >1 mM heme using Millipore centrifugal filter units (MW = 30,000; Millipore) at 7000 × *g* before freezing at −80 °C. As a means of quality assessment, absorbance spectra of oxy, deoxy, and CO derivatives were measured at 450–600 nm to confirm that the absorbance maxima of rHb mutants corresponded to those of the native Hbs. O_2-binding equilibria of rHb solutions were measured using the same protocol described above for the native Hb samples, and we used an enzymatic metHb reductase system (10) to maintain heme iron in the ferrous Fe^{2+} state. The measured P_{50} values for the native Hbs were based on pooled samples from multiple individuals per species, so allelic variation in the α- and β-chain subunits contributes to discrepancies in measured P_{50} values between the native Hbs, which have a heterogeneous amino acid composition, and the recombinant Hbs, which have an invariant amino acid composition.

Measurement of Epistasis. For the set of four rHb mutants representing each possible two-site combination of amino acid substitutions at β13 and β83, we tested for epistatic deviations from the expectations of an additive model: $\varepsilon = (P_{ii} + P_{jj}) - (P_{ij} + P_{ji})$, where P_{ij} is the measured P_{50} of the rHb with substitutions *i* and *j* at each site. The SE of the measured epistatic deviation, a linear function of P_{ij}, was calculated using the method of error propagation:

$\sigma_\varepsilon = \sqrt{\sigma P_{ii}^2 + \sigma P_{jj}^2 + \sigma P_{ij}^2 + \sigma P_{ji}^2}$, and the 95% confidence interval for ε was computed as $\varepsilon \pm \sigma_\varepsilon \times 1.96$ (11). Epistasis between a given pair of sites was considered to be statistically significant if the 95% confidence interval for ε did not include zero.

Phylogenetically Independent Contrasts. We used a four-gene DNA sequence alignment for 151 species of hummingbirds (12), augmented with 143 additional species and two additional nuclear genes to estimate an ultrametric phylogeny using BEAST (13), with branch-lengths scaled to relative time (Dataset S1). For the 10 species that were used in the experimental studies of Hb function, we calculated phylogenetically independent contrasts (PICs) of P_{50} values and regressed them against PICs of native elevation. All nodes in the phylogeny of these 10 focal species were resolved with 100% posterior probability. Elevational range data were primarily taken from Parker et al. (14). Results were consistent whether we used the maximum, midpoint, or minimum of the species' elevational range or the actual elevation at which the specimens were collected.

1. Weber RE (1981) Cationic control of oxygen affinity in lugworm erythocruorin. *Nature* 292(5821):386–387.
2. Weber RE (1992) Use of ionic and zwitterionic (Tris/BisTris and HEPES) buffers in studies on hemoglobin function. *J Appl Physiol (1985)* 72(4):1611–1615.
3. Weber RE, et al. (2004) Modulation of red cell glycolysis: Interactions between vertebrate hemoglobins and cytoplasmic domains of band 3 red cell membrane proteins. *Am J Physiol Regul Integr Comp Physiol* 287(2):R454–R464.
4. Imai K (1982) *Allosteric Effects in Haemoglobin* (Cambridge Univ Press, Cambridge, UK).
5. Mairbäurl H, Weber RE (2012) Oxygen transport by hemoglobin. *Compr Physiol* 2(2): 1463–1489.
6. Isaacks RE, et al. (1976) Studies on avian erythrocyte metabolism-IV. relationship between the major phosphorylated metabolic intermediates and oxygen affinity of whole blood in adults and embryos in several galliformes. *Comp Biochem Physiol A* 55(1):29–33.
7. Petschow D, et al. (1977) Causes of high blood O_2 affinity of animals living at high altitude. *J Appl Physiol* 42(2):139–143.
8. Maginniss LA (1985) Red cell organic phosphates and Bohr effects in house sparrow blood. *Respir Physiol* 59(1):93–103.
9. Natarajan C, et al. (2011) Expression and purification of recombinant hemoglobin in *Escherichia coli*. *PLoS ONE* 6(5):e20176.
10. Hayashi A, Suzuki T, Shin M (1973) An enzymic reduction system for metmyoglobin and methemoglobin, and its application to functional studies of oxygen carriers. *Biochim Biophys Acta* 310(2):309–316.
11. Natarajan C, et al. (2013) Epistasis among adaptive mutations in deer mouse hemoglobin. *Science* 340(6138):1324–1327.
12. McGuire JA, Witt CC, Altshuler DL, Remsen JV, Jr. (2007) Phylogenetic systematics and biogeography of hummingbirds: Bayesian and maximum likelihood analyses of partitioned data and selection of an appropriate partitioning strategy. *Syst Biol* 56(5): 837–856.
13. Drummond AJ, Rambaut A (2007) BEAST: Bayesian evolutionary analysis by sampling trees. *BMC Evol Biol* 7:214.
14. Parker TA, Stotz DF, Fitzpatrick JW (1996) in *Neotropical Bird Ecology and Conservation*, eds Parker TA, Moskovits DK (Univ Chicago Press, Chicago), pp. 113–436.

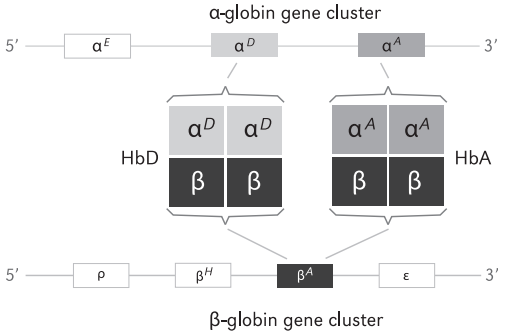

Fig. S1. Postnatally expressed Hb isoforms in avian red blood cells. The major isoform, HbA $(\alpha^A{}_2\beta_2)$, has α-type subunits encoded by the α^A-globin gene, and the minor isoform, HbD $(\alpha^D{}_2\beta_2)$, has α-type subunits encoded by the α^D-globin gene. Both isoforms share identical β-type subunits encoded by the β^A-globin gene. The remaining members of the α- and β-globin gene families (α^E-, ρ-, β^H, and ε-globin) are not expressed at appreciable levels in the definitive erythrocytes of adult birds. Within each gene cluster, the intergenic spacing is not drawn to scale.

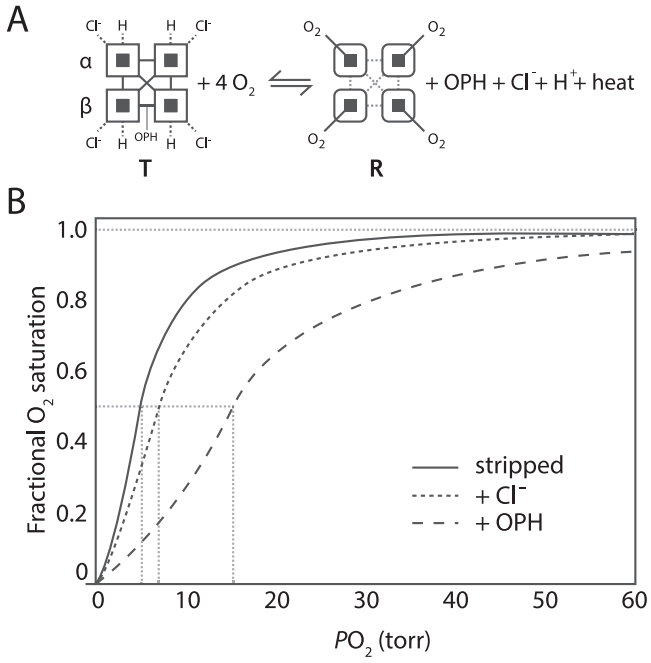

Fig. S2. Diagram illustrating the allosteric regulation of Hb-O_2 affinity. (*A*) The oxygenation reaction of tetrameric Hb ($\alpha_2\beta_2$) involves an allosteric transition in quaternary structure from the low-affinity T-state to the high-affinity R-state. The oxygenation-induced T→R transition entails a breakage of salt bridges and hydrogen bonds within and between subunits (open squares), dissociation of allosterically bound organic phosphates (OPHs), Cl^- ions, and protons, and the release of heat (heme oxygenation is an exothermic reaction). Deoxygenation-linked proton binding occurs at multiple residues in the α- and β-chains, Cl^- binding mainly occurs at the N-terminal α-amino groups of the α- and β-chains in addition to other residues in both chains, and phosphate binding occurs between the β-chains in the central cavity of the Hb tetramer. (*B*) O_2-equilibrium curves for purified Hb in the absence of allosteric effectors (stripped) and in the presence of chloride ions (+Cl^-) and organic phosphates (+OPH). The preferential binding of allosteric effectors to deoxyHb stabilizes the T-state, thereby shifting the allosteric equilibrium in favor of the low-affinity quaternary structure. The O_2-equilibrium curves are therefore right-shifted (Hb-O_2 affinity is reduced) in the presence of allosteric effectors. Hb-O_2 affinity is indexed by the P_{50} value, the PO_2 at which Hb is half-saturated. The sigmoidal shape of the O_2-equilibrium curves reflects cooperative O_2-binding, involving a PO_2-dependent shift from low- to high-affinity conformations.

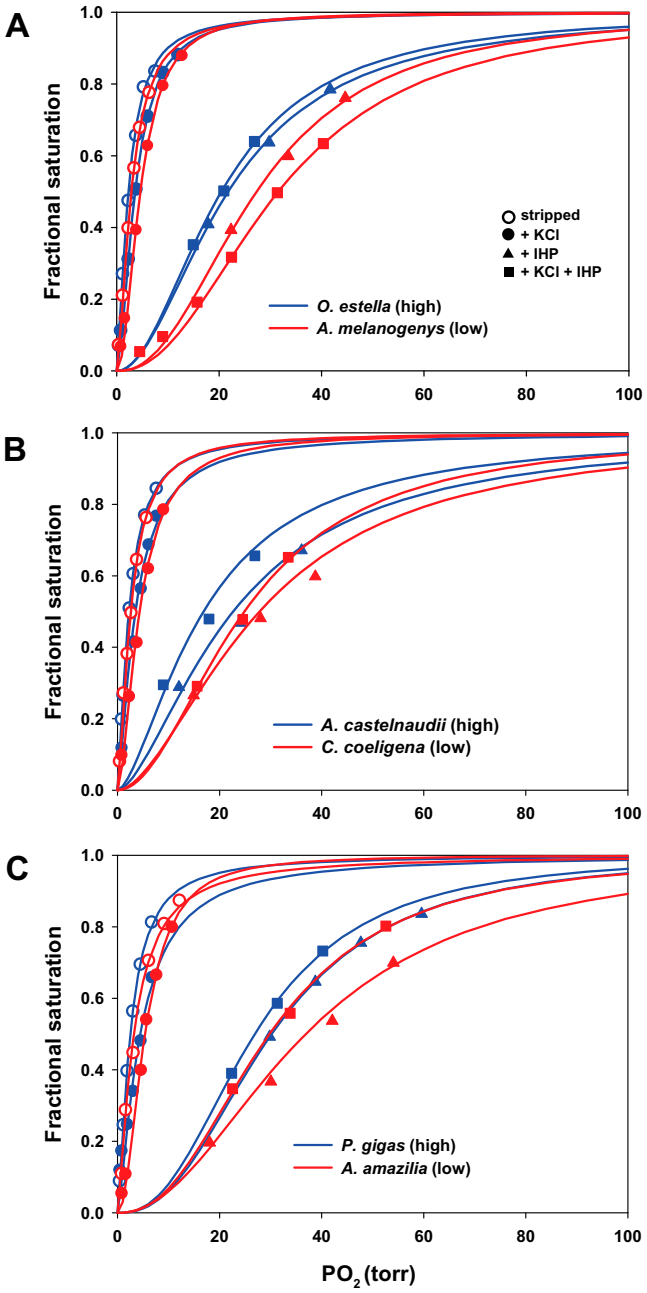

Fig. S3. O_2-equilibrium curves for purified HbA isoforms of high- and low-altitude hummingbird species. (*A*) Within the Coquettes, the Andean hillstar (*Oreotrochilus estella*), a montane species that occurs at elevations up to ~4,600 m, has a much higher Hb-O_2 affinity (i.e., a left-shifted O_2-equilibrium curve) relative to the speckled hummingbird (*Adelomyia melanogenys*), which is a middle-elevation species (1,000–2,900 m). (*B*) Within the Brilliants, the white-tufted sunbeam (*Aglaeactis castelnaudii*), a montane species that occurs at elevations up to ~4,600 m, has a much higher Hb-O_2 affinity relative to the bronzy Inca (*Coeligena coeligena*), which is native to the subtropical zone (1,000–2,200 m). (*C*) The giant hummingbird (*Patagona gigas*), which occurs at elevations up to ~4,300 m, has a higher Hb-O_2 affinity than the Amazilia hummingbird (*A. amazilia*), which is generally restricted to sea-level environments. See Table 1 for a summary of data on Hb function for all 10 species.

	α^A-globin										α^D-globin																β^A-globin					
	8	13	15	22	23	28	69	70	76	83	11	13	15	16	26	30	34	38	55	90	101	111	115	116	118	121	139	13	21	22	44	52	83
Common swift, *Apus apus*	T	V	A	E	A	A	A	A	I	L	Q	V	D	K	A	Q	T	Q	I	N	L	T	K	D	T	I	K	G	A	D	S	T	S
Adelomyia melanogenys	·	·	·	·	·	T	·	V	·	·	T	·	·	·	·	T	V	T	V	·	·	·	·	·	·	V	E	·	E	Q	·	·	G
Oreotrochilus estella	S	·	·	·	·	T	·	V	·	·	T	·	·	·	·	T	V	T	·	·	·	·	·	·	·	·	·	S	E	Q	·	·	·
Oreotrochilus melanogaster	S	·	·	·	·	T	·	V	·	·	T	·	·	·	·	T	V	T	·	·	·	·	·	·	·	·	·	S	E	Q	N	·	·
Aglaeactis castelnaudii	·	L	G	D	·	T	·	V	·	·	S	I	·	·	·	T	V	·	·	·	·	·	·	·	S	V	·	·	E	Q	·	·	·
Coeligena coeligena	·	L	G	·	·	·	·	·	·	·	S	·	·	·	V	T	V	·	·	D	P	·	E	G	S	V	·	·	E	Q	·	S	G
Coeligena violifer	·	L	G	·	·	·	·	V	M	·	S	I	·	R	·	T	V	·	·	·	·	·	·	·	S	V	·	·	E	Q	·	·	·
Patagona gigas	·	·	·	·	·	T	·	V	·	·	S	·	·	·	·	T	V	T	·	·	·	·	·	·	·	V	E	S	·	·	·	·	·
Amazilia viridicauda	·	I	·	·	D	T	·	V	·	·	T	I	E	·	·	T	V	·	V	·	·	·	·	·	·	V	·	·	·	·	·	·	·
Amazilia amazilia	·	I	·	·	D	T	·	V	·	·	T	I	E	·	·	A	V	·	V	·	·	·	·	·	·	V	·	·	·	E	·	·	G
Phaethornis malaris	·	I	·	·	D	T	P	V	·	F	A	I	·	·	·	T	A	·	V	·	·	S	·	E	·	V	·	·	·	E	·	·	G

Fig. S4. Variable residue positions in a multiple alignment of hummingbird globin sequences. Orthologous sequences from the common swift (*Apus apus*) are included for comparison. High-altitude species with maximum elevational ranges of >3,000 m are denoted by shading. Sequences represent the most common haplotypes for each species. Across all three adult-expressed globin genes (α^A-, α^D-, and β-globin), 33 of 428 amino acid sites are variable. Of the 33 variable sites, 12 have undergone repeated changes (parallelisms or reversals). Of those 12 sites, only β13 and β83 have undergone repeated amino acid replacements that are significantly associated with shifts in elevation (see text for details).

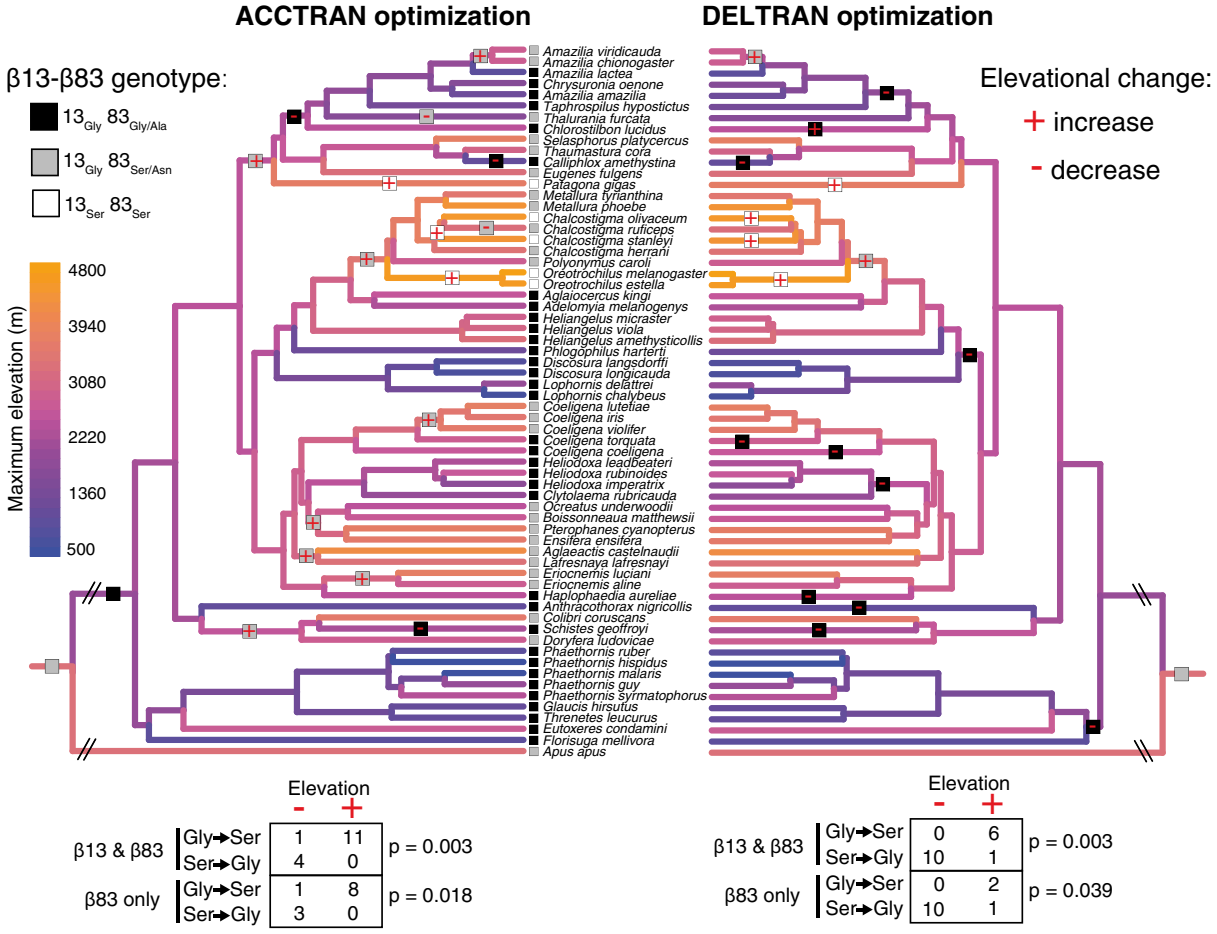

Fig. S5. Parsimony reconstructions reveal repeated substitutions and back-substitutions at β13 and β83 that are coincident with elevational range shifts during the diversification of Andean hummingbirds. Parsimony reconstructions of β13-β83 genotype were performed using accelerated (ACCTRAN) and delayed (DELTRAN) optimization to maximize reversals and parallel changes, respectively. The minimum number of transitions between Gly and Ser across the phylogeny of these 63 hummingbird species is 17, including 13 changes at β83 and 4 changes at β13. Regardless of the optimization scheme, Gly→Ser replacements at both sites are associated with upward shifts in elevation (+ symbols) relative to the immediate ancestor, whereas Ser→Gly replacements are associated with downward shifts in elevation (– symbols). In the ACCTRAN optimized scenario, the change that maps to the common ancestor of all hummingbirds is not associated with any inferred elevation change, which is why only 16 changes were included in the contingency table. Ancestral states for maximum elevation were estimated using maximum-likelihood.

Table S1. Linear regressions of Hb-O_2 affinity (P_{50}, torr) vs. native elevation for South American hummingbirds

		PIC		Nonphylogenetic	
X	Y	R^2	*P value*	R^2	*P value*
Midpoint elevation	HbA (stripped)	0.884	5.3×10^{-5}	0.842	1.8×10^{-4}
	HbA (+KCl)	0.538	0.016	0.796	0.001
	HbA (+IHP)	0.430	0.040	0.802	0.001
	HbA (+KCl+IHP)	0.737	0.001	0.651	0.005
	HbD (stripped)	0.877	0.019	0.820	0.034
	HbD (+KCl)	0.767	0.052	0.955	0.004
	HbD (+IHP)	0.890	0.016	0.851	0.026
	HbD (+KCl+IHP)	0.779	0.047	0.800	0.041
	HbA+HbD (stripped)	0.973	0.002	0.970	0.006
	HbA+HbD (+KCl)	0.928	0.008	0.887	0.017
	HbA+HbD (+IHP)	0.995	1.5×10^{-4}	0.995	1.4×10^{-4}
	HbA+HbD (+KCl+IHP)	0.983	9.7×10^{-4}	0.969	0.002
Maximum elevation	HbA (stripped)	0.800	4.7×10^{-4}	0.749	0.001
	HbA (+KCl)	0.497	0.023	0.754	0.001
	HbA (+IHP)	0.384	0.056	0.710	0.002
	HbA (+KCl+IHP)	0.581	0.010	0.512	0.020
	HbD (stripped)	0.978	0.001	0.949	0.005
	HbD (+KCl)	0.967	0.003	0.956	0.004
	HbD (+IHP)	0.987	0.001	0.974	0.002
	HbD (+KCl+IHP)	0.889	0.016	0.926	0.009
	HbA+HbD (stripped)	0.865	0.022	0.793	0.043
	HbA+HbD (+KCl)	0.947	0.005	0.904	0.013
	HbA+HbD (+IHP)	0.893	0.015	0.855	0.024
	HbA+HbD (+KCl+IHP)	0.787	0.045	0.714	0.072

Analysis of the HbA isoform was based on data from all 10 species, whereas the analysis of HbD and the weighted average of both isoforms (HbA+HbD) was based on data from a subset of five species (see main text for details). Coefficients of determination (R^2) and associated *P* values are given for regressions based on phylogenetically independent contrasts (PICs) and ordinary least-squares regressions that treat values for each species as independent datapoints. Results are shown for PIC and nonphylogenetic regressions using the midpoints and upper limits of the species-typical elevational ranges.

Table S2. Functional properties of recombinant hummingbird HbA mutants

	Stripped		+ IHP		+ KCl + IHP	
rHb mutant	P_{50}	n_{50}	P_{50}	n_{50}	P_{50}	n_{50}
β13Gly-β83Gly	2.74 ± 0.03	1.33 ± 0.04	24.22 ± 0.90	2.03 ± 0.17	19.38 ± 0.41	1.42 ± 0.07
β13Ser-β83Gly	3.21 ± 0.14	1.40 ± 0.03	13.79 ± 0.24	1.52 ± 0.10	10.99 ± 0.06	1.50 ± 0.11
β13Gly-β83Ser	3.08 ± 0.06	1.42 ± 0.02	16.73 ± 0.65	1.52 ± 0.10	11.76 ± 1.09	1.36 ± 0.06
β13Ser-β83Ser	3.21 ± 0.06	1.55 ± 0.07	24.70 ± 0.40	1.98 ± 0.08	16.31 ± 0.90	1.89 ± 0.11

O_2-affinities (P_{50}, torr) and cooperativity coefficients (n_{50}; mean ± SEM) measured in 0.1 M Hepes buffer at pH 7.40, 37 °C. Measurements were conducted in the absence of allosteric effectors (stripped), in the presence of IHP (IHP/Hb tetramer ratio = 2.0), and in the presence of both KCl (0.1 M) and IHP. [Heme], 0.3 mM.

Table S3. Variation among hummingbird β-globin variants in the nature of atomic contacts involving residue positions β13 and β83

Hb	Res 1	Res 2	CF	MF	SASA1	SASA2	Interaction
β13Gly-β83Gly	13G	15W	−0.215	−0.208	0.493	0.252	Short
	13G	16G	−0.818	−0.673	0.493	0.827	Short
	13G	17K	−0.910	−0.636	0.493	0.618	Water
	13G	18V	−1.324	0.792	0.493	0.107	Water
	13G	75V	−0.245	0.796	0.493	0.099	Water
	13G	126C	−0.875	0.763	0.493	0.048	Long
	83G	85F	−0.385	−0.315	0.613	0.028	Short
	83G	86A	−1.569	−1.227	0.613	0.432	Short
	83G	87Q	−1.113	−0.898	0.613	0.844	Water
	83G	89S	0.070	−0.766	0.613	0.020	Long
	83G	140A	−0.248	0.316	0.613	0.029	Long
	83G	143R	0.511	−0.895	0.613	0.440	Water
β13Ser-β83Ser	13S	15W	−0.172	−0.572	0.535	0.252	Water
	13S	16G	−1.223	−1.082	0.535	0.824	Water
	13S	17K	−0.874	−0.957	0.535	0.588	Water
	13S	121D	−1.203	−0.141	0.535	0.602	Water
	13S	126C	−0.560	0.680	0.535	0.048	Long
	83S	85F	−0.185	−0.399	0.631	0.028	Long
	83S	86A	−1.672	−1.011	0.631	0.427	Short
	83S	140A	−0.312	0.365	0.631	0.029	Long
β13Ser-β83Gly	13S	15W	−0.220	−0.573	0.535	0.252	Water
	13S	16G	−1.184	−1.102	0.535	0.824	Water
	13S	17K	−0.796	−0.949	0.535	0.588	Water
	13S	121D	−1.211	−0.141	0.535	0.602	Water
	13S	126C	−0.561	0.640	0.535	0.048	Long
	83G	85F	−0.429	−0.303	0.609	0.028	Short
	83G	86A	−1.571	−1.143	0.609	0.432	Short
	83G	87Q	−1.128	−0.934	0.609	0.844	Water
	83G	89S	−0.000	−0.811	0.609	0.020	Long
	83G	140A	−0.267	0.338	0.609	0.029	Long
	83G	143R	0.395	−0.854	0.609	0.440	Water
β13Gly-β83Ser	13G	15W	−0.199	−0.198	0.493	0.252	Short
	13G	16G	−0.847	−0.703	0.493	0.827	Short
	13G	17K	−0.863	−0.700	0.493	0.618	Water
	13G	18V	−1.247	0.736	0.493	0.107	Water
	13G	75V	−0.221	0.754	0.493	0.099	Water
	13G	126C	−0.821	0.844	0.493	0.048	Long
	83S	85F	−0.179	−0.404	0.631	0.028	Long
	83S	86A	−1.798	−1.148	0.631	0.429	Short
	83S	140A	−0.264	0.321	0.631	0.029	Long

β13Gly-β83Gly and β13Ser-β83Ser represent the wild-type genotypes of *A. melanogenys* and *O. estella*, respectively, and the other two genotypes represent mutational intermediates. Res 1 and 2 are identities of residues forming the contact (numbered from 1 to N). CF, configurational frustration index, which measures the interaction free energy for a given pair of native residues relative to the interaction free energies of all possible amino acid site-pairs in a similarly compact structure; MF, mutational frustration index, which measures the interaction free energy for a given pair of native residues relative to the interaction free energies between all possible amino acid site-pairs with the same coordinates; SASA1 and 2, solvent accessible surface area fractions for sites 1 and 2, respectively. Interaction: type of atomic contact: short range (short), long range (long), mediated by water molecule (water).

Table S4. Voucher specimens of South American hummingbirds used in the experimental analysis of Hb function

Species	Elevation (m)	NK tissue no.	MSB catalog number and direct Weblink to specimen data
Adelomyia melanogenys	1,395	161266	http://arctos.database.museum/guid/MSB:Bird:27492
Adelomyia melanogenys	1,395	161331	http://arctos.database.museum/guid/MSB:Bird:27552
Adelomyia melanogenys	2,102	163564	http://arctos.database.museum/guid/MSB:Bird:31892
Adelomyia melanogenys	2,111	163645	http://arctos.database.museum/guid/MSB:Bird:31973
Adelomyia melanogenys	2,052	163657	http://arctos.database.museum/guid/MSB:Bird:31985
Adelomyia melanogenys	2,144	163756	http://arctos.database.museum/guid/MSB:Bird:32084
Adelomyia melanogenys	2,147	163838	http://arctos.database.museum/guid/MSB:Bird:32166
Aglaeactis castelnaudii	4,470	159782	http://arctos.database.museum/guid/MSB:Bird:27124
Aglaeactis castelnaudii	4,330	159783	http://arctos.database.museum/guid/MSB:Bird:27125
Aglaeactis castelnaudii	4,030	159798	http://arctos.database.museum/guid/MSB:Bird:27140
Aglaeactis castelnaudii	4,330	159801	http://arctos.database.museum/guid/MSB:Bird:27143
Aglaeactis castelnaudii	4,470	159808	http://arctos.database.museum/guid/MSB:Bird:27149
Aglaeactis castelnaudii	4,300	159809	http://arctos.database.museum/guid/MSB:Bird:27150
Aglaeactis castelnaudii	4,578	169373	http://arctos.database.museum/guid/MSB:Bird:34147
Amazilia amazilia	366	162007	http://arctos.database.museum/guid/MSB:Bird:27595
Amazilia amazilia	366	162009	http://arctos.database.museum/guid/MSB:Bird:27597
Amazilia amazilia	366	162020	http://arctos.database.museum/guid/MSB:Bird:27604
Amazilia amazilia	366	162024	http://arctos.database.museum/guid/MSB:Bird:27608
Amazilia amazilia	366	162026	http://arctos.database.museum/guid/MSB:Bird:31222
Amazilia amazilia	366	162027	http://arctos.database.museum/guid/MSB:Bird:31223
Amazilia amazilia	352	163017	http://arctos.database.museum/guid/MSB:Bird:31453
Amazilia amazilia	132	168989	http://arctos.database.museum/guid/MSB:Bird:33763
Amazilia amazilia	115	169303	http://arctos.database.museum/guid/MSB:Bird:34077
Amazilia viridicauda	3,005	159899	http://arctos.database.museum/guid/MSB:Bird:27227
Amazilia viridicauda	3,005	159900	http://arctos.database.museum/guid/MSB:Bird:27228
Amazilia viridicauda	3,005	159901	http://arctos.database.museum/guid/MSB:Bird:27229
Amazilia viridicauda	2,953	168478	http://arctos.database.museum/guid/MSB:Bird:33259
Amazilia viridicauda	2,953	168480	http://arctos.database.museum/guid/MSB:Bird:33261
Amazilia viridicauda	2,900	168488	http://arctos.database.museum/guid/MSB:Bird:33269
Amazilia viridicauda	2,953	168493	http://arctos.database.museum/guid/MSB:Bird:33274
Coeligena coeligena	2,052	163658	http://arctos.database.museum/guid/MSB:Bird:31986
Coeligena coeligena	2,052	163741	http://arctos.database.museum/guid/MSB:Bird:32069
Coeligena coeligena	2,131	163914	http://arctos.database.museum/guid/MSB:Bird:32242
Coeligena coeligena	2,100	163915	http://arctos.database.museum/guid/MSB:Bird:32243
Coeligena coeligena	2,052	167517	http://arctos.database.museum/guid/MSB:Bird:32345
Coeligena coeligena	2,240	167534	http://arctos.database.museum/guid/MSB:Bird:32362
Coeligena coeligena	2,052	167823	http://arctos.database.museum/guid/MSB:Bird:32651
Coeligena violifer	2,798	163129	http://arctos.database.museum/guid/MSB:Bird:31564
Coeligena violifer	2,778	163210	http://arctos.database.museum/guid/MSB:Bird:31645
Coeligena violifer	2,810	163213	http://arctos.database.museum/guid/MSB:Bird:31648
Coeligena violifer	3,710	163485	http://arctos.database.museum/guid/MSB:Bird:31813
Coeligena violifer	2,858	168451	http://arctos.database.museum/guid/MSB:Bird:33232
Coeligena violifer	3,688	169121	http://arctos.database.museum/guid/MSB:Bird:33895
Coeligena violifer	3,688	169124	http://arctos.database.museum/guid/MSB:Bird:33898
Coeligena violifer	3,779	169232	http://arctos.database.museum/guid/MSB:Bird:34006
Oreotrochilus estella	4,363	169336	http://arctos.database.museum/guid/MSB:Bird:34110
Oreotrochilus estella	4,391	169357	http://arctos.database.museum/guid/MSB:Bird:34131
Oreotrochilus estella	4,512	169396	http://arctos.database.museum/guid/MSB:Bird:34170
Oreotrochilus melanogaster	3,840	163409	http://arctos.database.museum/guid/MSB:Bird:31737
Oreotrochilus melanogaster	3,750	163419	http://arctos.database.museum/guid/MSB:Bird:31747
Oreotrochilus melanogaster	3,974	168616	http://arctos.database.museum/guid/MSB:Bird:33397
Oreotrochilus melanogaster	4,150	168641	http://arctos.database.museum/guid/MSB:Bird:33422
Oreotrochilus melanogaster	4,088	168649	http://arctos.database.museum/guid/MSB:Bird:33430
Oreotrochilus melanogaster	4,082	168655	http://arctos.database.museum/guid/MSB:Bird:33436
Oreotrochilus melanogaster	4,140	168656	http://arctos.database.museum/guid/MSB:Bird:33437
Patagona gigas	3,360	159890	http://arctos.database.museum/guid/MSB:Bird:27221
Patagona gigas	3,967	163090	http://arctos.database.museum/guid/MSB:Bird:31526
Patagona gigas	3,967	163099	http://arctos.database.museum/guid/MSB:Bird:31535
Patagona gigas	3,973	163100	http://arctos.database.museum/guid/MSB:Bird:31536
Patagona gigas	3,973	163108	http://arctos.database.museum/guid/MSB:Bird:31544
Patagona gigas	3,750	163373	http://arctos.database.museum/guid/MSB:Bird:31701
Patagona gigas	3,750	163391	http://arctos.database.museum/guid/MSB:Bird:31719
Patagona gigas	4,082	168693	http://arctos.database.museum/guid/MSB:Bird:33474

Table S4. Cont.

Species	Elevation (m)	NK tissue no.	MSB catalog number and direct Weblink to specimen data
Phaethornis malaris	353	162160	http://arctos.database.museum/guid/MSB:Bird:27711
Phaethornis malaris	350	162199	http://arctos.database.museum/guid/MSB:Bird:27743
Phaethornis malaris	360	162253	http://arctos.database.museum/guid/MSB:Bird:31267
Phaethornis malaris	323	162297	http://arctos.database.museum/guid/MSB:Bird:31273
Phaethornis malaris	365	162333	http://arctos.database.museum/guid/MSB:Bird:27859
Phaethornis malaris	317	162362	http://arctos.database.museum/guid/MSB:Bird:27883

The listed Weblinks to the Museum of Southwestern Biology (MSB) online catalog provide detailed locality information and ancillary data for each of the 70 specimens.

Other Supporting Information Files

Dataset S1 (PDF)